Published online 22 September 2021 *Nucleic Acids Research, 2021, Vol. 49, No. 18* ***10493–10506***
https://doi.org/10.1093/nar/gkab777

Replication-dependent cytotoxicity and Spartan-mediated repair of trapped PARP1–DNA complexes

Liton Kumar Saha[1], Yasuhisa Murai[1], Sourav Saha[1], Ukhyun Jo[1], Masataka Tsuda[2,3], Shunichi Takeda[2] and Yves Pommier[1,*]

[1]Developmental Therapeutics Branch & Laboratory of Molecular Pharmacology, Center for Cancer Research, National Cancer Institute, NIH, Bethesda, MD 20892, USA, [2]Department of Radiation Genetics, Kyoto University, Graduate School of Medicine, Yoshida Konoe, Sakyo-ku, Kyoto 606-8501, Japan and [3]Program of Mathematical and Life Sciences, Graduate School of Integrated Sciences for Life, Hiroshima University, Higashi-Hiroshima 739-8526, Japan

Received January 20, 2021; Revised July 28, 2021; Editorial Decision August 24, 2021; Accepted September 02, 2021

ABSTRACT

The antitumor activity of poly(ADP-ribose) polymerase inhibitors (PARPis) has been ascribed to PARP trapping, which consists in tight DNA–protein complexes. Here we demonstrate that the cytotoxicity of talazoparib and olaparib results from DNA replication. To elucidate the repair of PARP1–DNA complexes associated with replication in human TK6 and chicken DT40 lymphoblastoid cells, we explored the role of Spartan (SPRTN), a metalloprotease associated with DNA replication, which removes proteins forming DPCs. We find that SPRTN-deficient cells are hypersensitive to talazoparib and olaparib, but not to veliparib, a weak PARP trapper. SPRTN-deficient cells exhibit delayed clearance of trapped PARP1 and increased replication fork stalling upon talazoparib and olaparib treatment. We also show that SPRTN interacts with PARP1 and forms nuclear foci that colocalize with the replicative cell division cycle 45 protein (CDC45) in response to talazoparib. Additionally, SPRTN is deubiquitinated and epistatic with translesion synthesis (TLS) in response to talazoparib. Our results demonstrate that SPRTN is recruited to trapped PARP1 in S-phase to assist in the excision and replication bypass of PARP1–DNA complexes.

INTRODUCTION

The genome is constantly subjected to DNA damage, including DNA–protein crosslinks (DPCs), which are produced by enzymatic and non-enzymatic mechanisms (1,2). When DNA topoisomerases, DNA methyltransferases (DNMT), DNA polymerases (Polβ) and poly(ADP-ribose) polymerase 1 (PARP1) form catalytic intermediates, such reaction intermediates can become trapped on DNA, thereby forming tight enzyme-DNA complexes (2–10). In addition to non-covalent PARP1 trapping (11,12), crosslinking of PARP1 at the 3′-end of breaks made by AP endonuclease has been reported (4).

PARP1 is abundant in chromatin and acts as a multifaceted enzyme regulating a range of cellular processes including DNA damage sensing, DNA repair, chromatin remodeling and transcription (12,13). PARP1 is activated after binding to DNA single- and double-strand breaks (SSBs and DSBs) to catalyze PARylation of itself and various proteins involved in DNA metabolism especially base excision repair (BER) enzymes, which facilitates their assembly (13). PARP1 has been reported to be associated with DNA replication (14,15), to form replication foci in S phase (16) and to be present at replication forks and interact with proteins involved in DNA replication (17–19). PARP1 has been described as a sensor of unligated Okazaki fragments to facilitate their ligation (20). PARP1 can also affect replication fork progression on damaged DNA (21), restart stalled replication forks (22) and stabilize replication forks by inhibiting their restart by RECQ1 helicase (23). A recent study also identified CARM1 as a regulator of PARP1 activity promoting replication fork reversal, thus maintaining replication fork speed and fidelity (24).

PARP inhibitors (PARPis) including olaparib, talazoparib, niraparib and rucaparib are cancer chemotherapeutics that kill cancer cells by trapping PARP1 (11,12,25,26). Trapped PARP1 appears to be so tightly bound to DNA that it results in a DPC-like lesion that requires homologous recombination repair for resolution (11,12,27–29). These PARP1–DNA complexes interfere with DNA transactions and may lead to replication fork

*To whom correspondence should be addressed. Tel: +1 240 760 6142; Fax: +1 240 541 4475; Email: Yves.Pommier@nih.gov

Published by Oxford University Press on behalf of Nucleic Acids Research 2021.
This work is written by (a) US Government employee(s) and is in the public domain in the US.

stalling, checkpoint activation and apoptosis (12,30) as a single unrepaired DSB can activate programmed cell death pathways (31,32).

Proteolytic degradation of DPCs in replisomes has been shown to be catalyzed both by proteasomes or SPRTN (33). SPRTN, a DNA-dependent metalloprotease and a functional homolog of yeast Wss1, proteolyzes DPCs in a replication-coupled manner (34,35). Germline mutations in the *SPRTN* gene cause Ruijs-Aalfs syndrome (RJALS) characterized by premature aging, early onset hepatocellular carcinoma and chromosomal instability (36,37). Likewise, hypomorphic SPRTN mice recapitulate the RJALS patient phenotypes, namely progeria and liver tumorigenesis (38). Loss of SPRTN causes lethality across a wide spectrum of mammalian cell lines and embryonic lethality in mice, which highlights the importance of SPRTN for handling DNA lesions, and particularly DPCs (38–40). The catalytic domain (sprT domain) of SPRTN contains a ZBD subdomain and BR regions responsible for its binding to DNA (41,42). SPRTN is activated by DNA featuring both single- and double-stranded segments (34,35,41,43). SPRTN has a wide range of substrates including histones, topoisomerases and other chromatin-bound proteins (43,44). Given that SPRTN is a constitutive part of the replisome (35), we reasoned that SPRTN might have role in degrading PARP-DNA complexes in addition to the proteasome, which has been shown to repair trapped PARP1 in murine cells (4,45). Considering the redundancy of the DPC repair pathways (10), it is plausible that different cellular mechanisms exist to remove trapped PARPs in chromatin.

Here, we demonstrate that both human and chicken *SPRTN*-knockout cells are hypersensitive to PARP inhibitors that trap PARP1, exhibit elevated levels of PARP1–DNA complexes after talazoparib treatment and delayed repair of PARP1–DNA complexes following withdrawal of talazoparib. We also show that SPRTN forms nuclear foci, interacts with PARP1, and prevents slowing down of replication forks upon PARP trapping. We conclude that SPRTN facilitates the repair of the bulky PARP1–DNA lesions generated by PARP inhibitors in chromatin as a replication-associated protease.

MATERIALS AND METHODS

Cell lines, culture conditions and transfection

Human TK6 B cells were cultured in RPMI1640 medium (Cat# 11-875-093, Gibco, US) supplemented with horse serum (5%, Gibco, USA), penicillin (100 U/ml), streptomycin (100 μg/ml, ThermoFischer, USA), and sodium pyruvate (200 mg/ml, ThermoFischer, USA) and maintained at 37°C under a humidified atmosphere and CO_2 (5%). *PARP1*$^{-/-}$ and *SPRTN*$^{-/-}$TK6 cells were generated by CRISPR/Cas9 method (46,47). To generate double mutant of *SPRTN*$^{-/-}$/*PARP1*$^{-/-}$, two targeting vectors and pX330-gRNA (the gRNA was inserted into the BbsI site of pX330 vector (Cat# 42230, Addgene, US) targeting PARP1 (47) were transfected into *SPRTN*$^{-/-}$ TK6 cells. Chicken DT40 cells were cultured as described (48). Deletion of SPRTN in DT40 cells was carried out as described previously (48). Transfection of expression vectors (EGFP tagged SPRTN WT and SPRTN E112A) was carried-out using Lipofectamine 3000 (ThermoFischer, US) reagents as per the protocol from the manufacturer.

Cell viability assays

To measure the sensitivity of TK6 and DT40 cells, we conducted colony formation assays by counting colony formation in methylcellulose plates as described (49). Briefly, after overnight mixing of drugs with methylcellulose-containing medium overnight at 4°C or for the times indicated in the figure legends, drug-containing media were plated on 6-well cluster plates in 5 ml per well. Serially diluted TK6 and DT40 cells were then seeded onto triplicate wells of six-well cluster plates in 5 ml per well of D-MEM/F-12 (Life Technologies) supplemented with 10% horse serum, 2 mM L-glutamine, 200 μg/ml sodium pyruvate and 1.5% (w/v) methylcellulose (Sigma). We counted colonies 10–14 days after drug treatments and the percentage of surviving colonies was expressed relative to the percentage of untreated colonies.

Measurement of PARP1 trapping in genomic DNA

The chromatin-bound subcellular fractions were prepared according to the protocol of Subcellular Protein Fractionation Kit from Thermo Scientific (78840) following immunoblotting with PARP1 antibody. Delails of this assay have been described previously (11).

Western blotting

Cells (1×10^6) were lysed in 100 μl sodium dodecyl sulfate (SDS) buffer containing Tris–HCl (25 mM, pH 6.5), SDS (1%), β-mercaptoethanol (0.24 mM), bromophenol blue (0.1%) and glycerol (5%). Whole-cell extracts were separated by electrophoresis, transferred onto polyvinylidene difluoride membranes and blocked in 5% skimmed milk dissolved in Tween-20 (0.1%) containing phosphate buffer saline (PBS). Membranes were incubated with primary antibodies overnight at 4°C followed by washing in Tween-20 (0.1%) in PBS. Membranes were incubated with appropriate HRP-linked secondary antibodies at room temperature for 1 h and washed twice, and were developed by chemiluminescence with ECL reagent.

Immunoprecipitation

Cells pellets were incubated on ice for 15 min in pre-extraction buffer (25 mM HEPES, pH 7.4, 50 mM NaCl, 1 mM EDTA, 3 mM $MgCl_2$, 300 mM sucrose, 0.5% Triton-X-100), supplemented with protease and phosphatase inhibitors. After centrifugation (5000 g, 5 min) and removal of the supernatant, chromatin pellets were resuspended in RIPA buffer (10 mM Tris–HCl pH7.5, 150 mM NaCl, 5 mM EDTA, 0.1% SDS, 1% Triton-X-100, 1% sodium deoxycholate) supplemented with protease and phosphatase inhibitors. Lysates were homogenized and incubated with benzonase for 1 h on a rotator at 4°C. After centrifugation (18 000 × g, 10 min), the supernatant was collected and used for protein concentration measurement. 300 μg of the

extract were resuspended in 200 μl RIPA buffer and 100 μl dilution/washing buffer (10 mM Tris–HCl pH7.5, 150 mM NaCl, 5 mM EDTA) supplemented with protease and phosphatase inhibitors. Samples were then incubated with 2 μg of anti-EGFP antibody (Abcam, ab184601) on a rotator overnight at 4°C. Protein G agarose beads were washed three times for 5 min with washing buffer and incubated with the samples for 3 h on a rotator at 4°C. After three washes, proteins were eluted with loading buffer and incubated for 5 min at 95°C on a thermomixer. After centrifugation at 18 000 g (1 min), supernatants were transferred to new tubes, and the proteins separated by electrophoresis.

Immunofluorescence

To visualize EGFP-tagged SPRTN and CDC45 foci, cells were plated in 6-well plates on sterilized coverslips and treated the next day with either DMSO as a vehicle or with 1 μM talazoparib for 1 h. After washing with cold PBS, pre-extraction was performed with CSK buffer (10 mM HEPES–KOH pH7.4, 300 mM sucrose, 100 mM NaCl and 3 mM $MgCl_2$) supplemented with 0.5% Triton X-100 for 10 min on ice followed by fixation in 4% paraformaldehyde in PBS for 15 min at room temperature. Blocking was done in 3% BSA/PBS for 30 min prior to washing with PBS. Coverslips were incubated for 2 h with the primary antibodies (Anti-EGFP antibody, ab184601, mouse, diluted 1:500; Anti-CDC45 antibody, Cell Signalling 11881S, rabbit, diluted 1:100) in 3% BSA/PBS in a humid chamber. After washing with cold PBS, incubation with secondary antibodies (AlexaFluor 568, A11036, goat anti-rabbit, diluted 1:100; AlexaFluor 488, A11029, goat anti-mouse, diluted 1:1000) lasted 1 h in the dark in a humid chamber. Mounting medium with DAPI (VECTASHIELD, Vector Laboratories) was added after the last wash. Images were captured with a Zeiss LSM 880 super resolution microscope with 63× objective lens.

DNA combing

We measured replication fork progression as described with some modifications (50–52). Briefly, cells were labeled with 100 μM CldU (Sigma) for 30 min, washed three times with pre-warmed PBS, and labeled with 100 μM IdU (Sigma) for an additional 30 min. After labeling with IdU, cells were immediately washed three times with ice-cold PBS to inhibit DNA replication. The IdU labeling was performed in the absence or presence of 1 μM talazoparib, 10 μM Olaparib or 10 μM veliparib. Cells were collected, resuspended in PBS and lysed with lysis buffer (200 mM Tris–HCl pH 7.4, 50 mM EDTA, 0.5% SDS). DNA fibers were extracted in agarose plugs and stretched onto silanized coverslips. Combed DNA was dehydrated in an oven at 60°C for 2 h and denatured with 0.4 M NaOH for 20 min. Samples were washed three times with PBS for 5 min each time on a shaker, dehydrated sequentially in 70, 90 and 100% ethanol for 2 min each and dried at room temperature for 10 min. Samples were blocked with 0.5% BSA in PBS containing 0.1% TritonX-100 (PBST) for 30 min and incubated with rat and mouse anti-BrdU antibodies recognizing CldU and IdU, respectively at 4°C for overnight. After washing with PBST, anti-mouse Cy3 and anti-rat Cy5 were used as secondary antibodies. After washing with PBST, samples were mounted with ProLong Gold. DNA fibers were photographed on a Zeiss fluorescent microscope and the length of CldU and IdU tracts were measured using FiberStudio 2.0 software.

Alkaline-comet assays

Alkaline-comet assay (also known as the single-cell gel electrophoresis assay) was used to quantify SSBs, as described (53). The quantification of tail moments was done with the CometScore software.

Quantification and statistical analyses

Western blots were quantiied using ImageJ (Fiji) and statistical analyses were carried out using GraphPad prism 8 software. Test methods are described in each figure legend. $*P < 0.05$, $**P < 0.01$, $***P < 0.001$, $****P < 0.0001$ was considered significant and ns = not significant.

RESULTS

DNA replication-dependent cytotoxicity of talazoparib

To determine whether PARPi cytotoxicity is dependent on DNA replication, first we performed colony survival assays using human lymphoblastoid TK6 cells after short-term (30 min) treatments with talazoparib, over a wide concentration range (0.01–100 nM) (Figure 1A). Under these conditions, TK6 cells showed minimal (10%-15%) cytotoxicity in response to pharmacological concentrations of talazoparib (Figure 1A). To test the potential role of replication fork collisions in the cytotoxicity of talazoparib, we next performed the colony survival assays following exposure to fixed therapeutic concentration (10 nM) of talazoparib for different times. Cell killing increased with the time of exposure to talazoparib (Figure 1B), which is reminiscent of the replication-dependent cytotoxicity of topoisomerase I inhibitors (54).

We next asked whether replication inhibition could affect the cellular cytotoxicity to PARPis. To this end, we pretreated cells with the DNA polymerase inhibitor aphidicolin for a short time (10 min) followed by up to two hours co-treatment of talazoparib and aphidicolin. Aphidicolin protected the cells from talazoparib (Figure 1C). These experiments suggested that the cytotoxicity of talazoparib requires active DNA replication.

SPRTN$^{-/-}$ cells are selectively hypersensitive to potent PARP trappers

As SPRTN repairs DPCs in a DNA replication-coupled manner (33,35), we hypothesized that SPRTN might repair the DPC-like lesions produced by PARP-DNA complexes. To evaluate this possibility, we performed colony survival assays in *SPRTN* $^{-/-}$ TK6 cells (46). As expected, the *SPRTN* $^{-/-}$ TK6 cells were hypersensitive to the classical DPC-inducing agents; the crosslinking agent cisplatin,

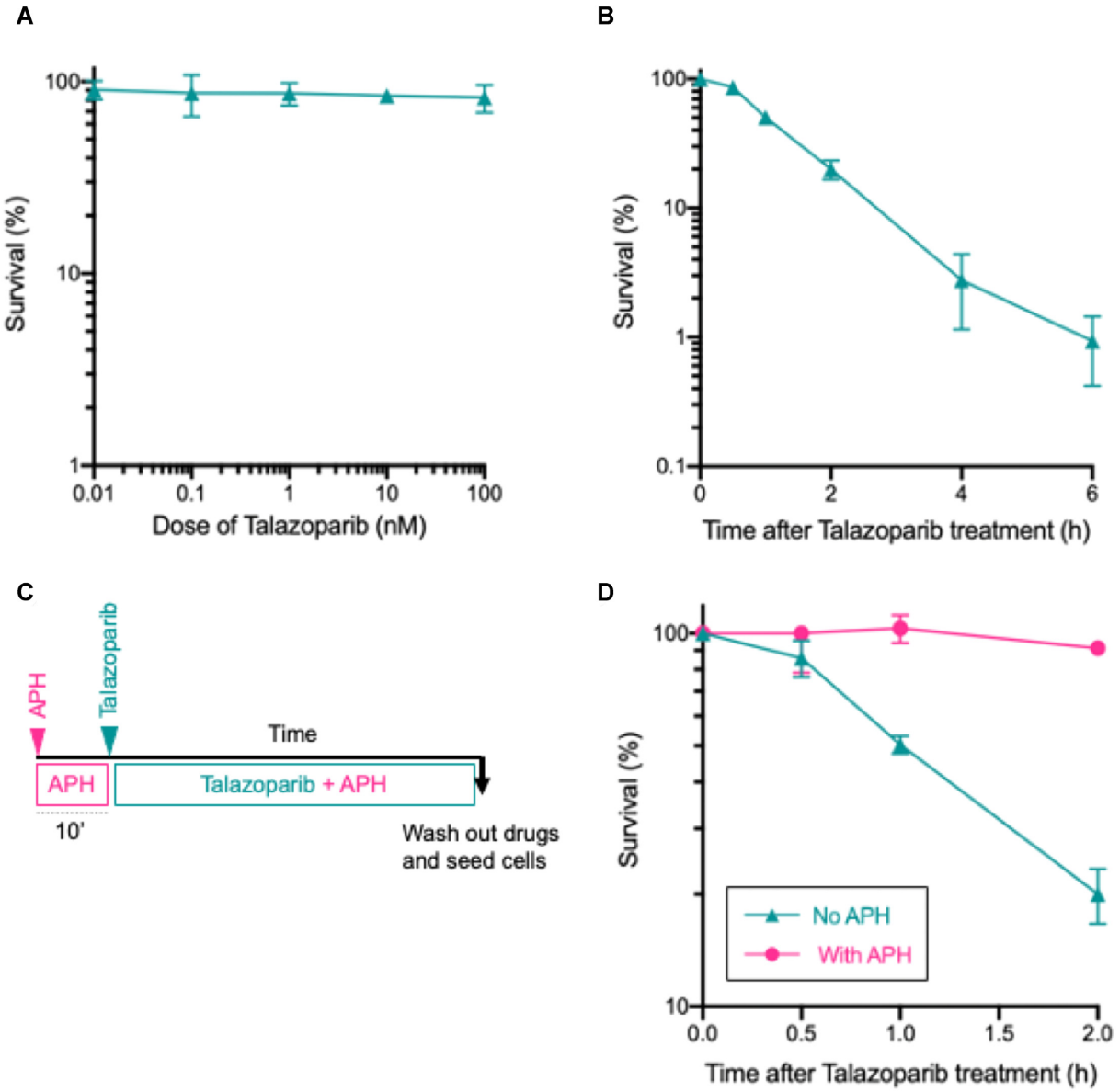

Figure 1. Time- and replication-dependent cytotoxicity of talazoparib in human lymphoblastoid TK6 cells measured by colony formation assays. (**A**) Limited cytotoxicity of 30-min talazoparib treatments. The concentration of talazoparib is displayed on the x-axis and the fraction of surviving cells on the y-axis in a logarithmic scale. (**B**) Time-dependent cytotoxicity of talazoparib. Cells were treated with 10 nM talazoparib for the indicated times. (**C**) Treatment protocol for the experiments shown in panel D. TK6 cells were pretreated with aphidicolin (APH) for 10 min followed by talazoparib treatment for the indicated times while keeping APH in the culture. (**D**) Aphidicolin prevents talazoparib-induced cytotoxicity. Cells were either treated with talazoparib alone or talazoparib plus APH (1 μM). Error bars indicate SD of mean for three independent experiments.

the topoisomerase I (TOP1) poison camptothecin and the TOP2 poison etoposide (Supplementary Figure S1A-C) (35,43,55).

We next tested the sensitivity of our *SPRTN* $^{-/-}$ TK6 cells to PARP inhibitors with differential PARP trapping ability (11,12). *SPRTN* $^{-/-}$ cells were hypersensitive to talazoparib and olaparib (Figure 2A & B) but not to veliparib, a weak PARP trapper (11) (Figure 2C). To verify that the observed phenotype was not restricted solely to this cell line, we repeated the colony survival assays with DT40 chicken lymphoblast cells, in which SPRTN was knocked-out using CRISPR-Cas9. Like TK6 cells, the *SPRTN* $^{-/-}$ DT40 cells were hypersensitive to both talazoparib and olaparib (Figure 2D and E) but not to veliparib (Figure 2F). The phenotypic similarity between *SPRTN* $^{-/-}$ TK6 and DT40 cells suggests the implication of SPRTN in the cellular tolerance to PARP trappers.

Depletion of PARP1 in *wild-type* and *SPRTN* $^{-/-}$ TK6 cells (Supplementary Figure S2B) conferred resistance to both talazoparib and olaparib (Figure 2G and H), indicating that the hypersensitivity of the *SPRTN* $^{-/-}$ TK6 cells is dependent on PARP trapping. Conversely, ectopic expression of SPRTN in *SPRTN* $^{-/-}$ TK6 cells (Supplementary Figure S2A) restored the talazoparib sensitiv-

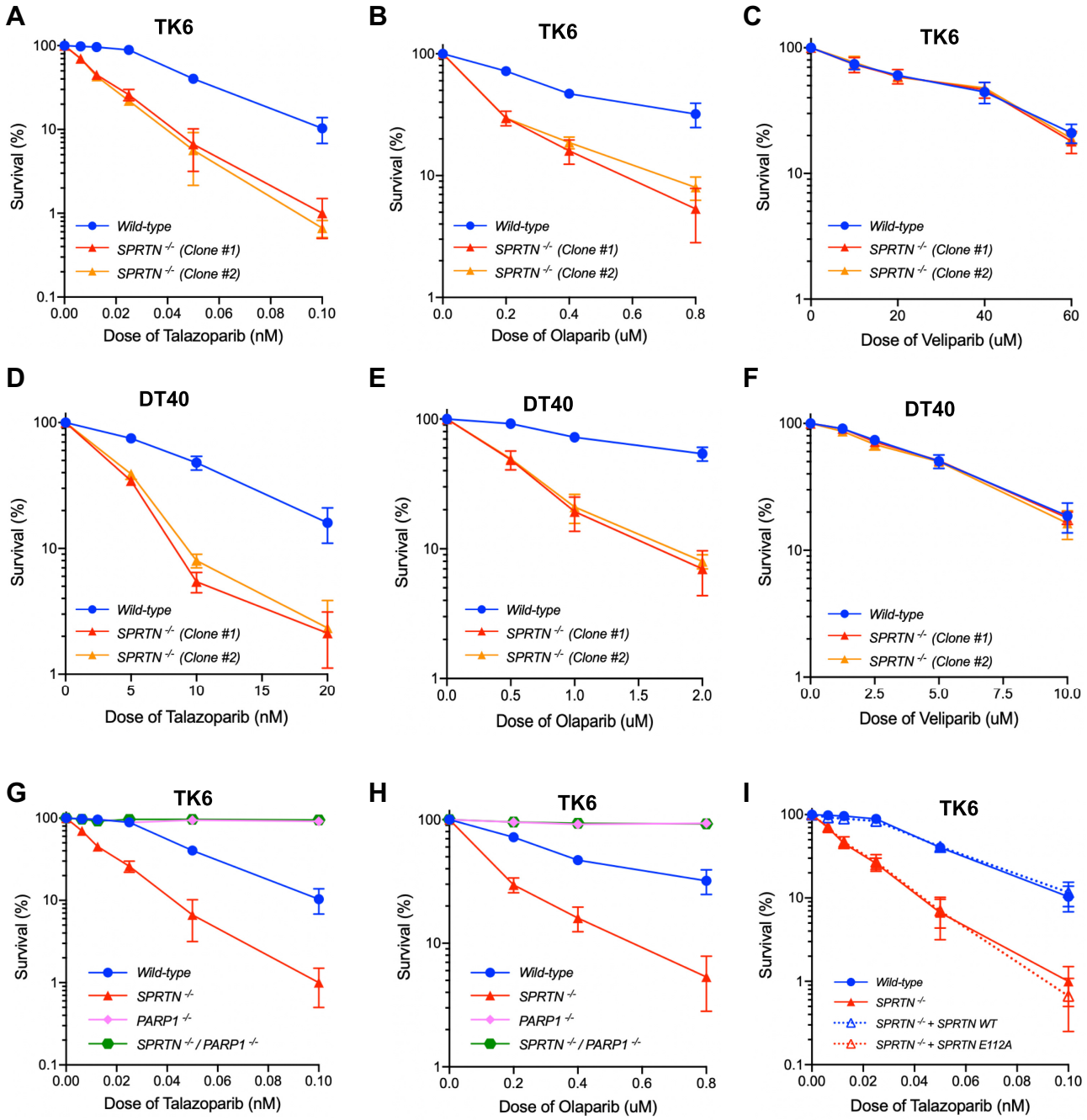

Figure 2. Hypersensitivity of mammalian *SPRTN*$^{-/-}$ cells to PARP trappers. Colony survival of human TK6 (**A–C** and **G–I**) and chicken DT40 cells (**D–F**) carrying the indicated genotypes following exposure to PARPis: talazoparib (A and D), olaparib (B and E) and veliparib (C and F). The drug concentrations are displayed on the x-axis on a linear scale, and the percentage of surviving cells displayed on the y-axis in logarithmic scale. Error bars show the SD of mean for three independent experiments. Percent survival was calculated as the percentage of drug-treated surviving cells relative to the untreated surviving cells.

ity to a similar level as in *wild-type* cells whereas expression of SPRTN E112A (Supplementary Figure S2A) that is deficient of its metalloprotease activity failed to protect the cells from talazoparib (Figure 2I). These data indicate that the catalytic activity of SPRTN determines the cellular resistance to PARP trappers in the cell lines examined.

Accumulation and persistence of PARP1–DNA complexes in SPRTN KO TK6 and DT40 cells

To test whether PARP1–DNA complexes caused the hypersensitivity of *SPRTN*$^{-/-}$ cells, we measured the levels of PARP1–DNA complexes (PARP1 trapping) by fractionating cell lysates into chromatin-bound fractions after pulse-exposure of cells to talazoparib in the presence of methyl

methanesulfonate (MMS), which enhances and facilitates the quantitation of PARP trapping (11). *Wild-type and SPRTN*$^{-/-}$ TK6 and DT40 cells both exhibited enhanced PARP1 trapping (Figure 3A & B). Chromatin trapping of PARP1 was observed as early as 10 min in talazoparib-treated cells, and accumulation of PARP1 in chromatin fractions was higher (∼2-fold) both in the *SPRTN*$^{-/-}$ TK6 and DT40 cells than in their *wild-type* counterparts (Figure 3A and B).

To assess the implication of SPRTN in the removal of PARP1–DNA complexes, we monitored the repair kinetics of PARP1–DNA complexes after pulse-exposure of *wild-type and SPRTN*$^{-/-}$ cells with talazoparib and MMS and followed the recovery of PARP1–DNA complexes in drug-free medium. Almost 90% of the talazoparib-induced PARP1–DNA complexes were removed within 1 hour in *wild-type* TK6 cells (Figure 3C). However, *SPRTN*$^{-/-}$ TK6 cells showed delayed removal of PARP1–DNA complexes in comparison with *wild type* cells (Figure 3C). A similar phenotype was observed in chicken DT40 cells (Figure 3D). These data indicate that SPRTN is required for the elimination of PARP1–DNA complexes and in mitigating the toxicity of PARPis. To eliminate the possibility that the increased PARP1 trapping in *SPRTN*$^{-/-}$ cells could be due to increased levels of MMS-induced SSBs that could induce more PARP1 trapping, we performed alkaline comet assay to measure MMS-induced SSBs and their recovery after washing out MMS. The *wild-type* and *SPRTN*$^{-/-}$ TK6 cells both displayed similar SSBs, excluding the possible role of SPRTN in BER (Supplementary Figure S3A). These data suggest that the increased induction and delayed repair of trapped PARP1 in *SPRTN*$^{-/-}$ cells are dependent on SPRTN for the processing of trapped PARP1.

To examine how much trapped PARP1 is processed by SPRTN, we compared the levels of trapped PARP1 after subcellular cell fractionations in *wild-type* and *SPRTN* KO TK6 cells relative to the total nuclear abundance of PARP1 in these cells. After 30-min treatments with 10 nM talazoparib, *wild-type* cells showed that ∼30% of nuclear PARP1 was trapped whereas SPRTN-deficient cells showed the trapping of ∼45% of its total nuclear PARP1 (Supplementary Figure S3B). These data suggest that ∼15% of trapped PARP1 is processed by SPRTN.

SPRTN prevents replication fork stalling by PARP inhibitors

Because SPRTN is localized at replication forks and plays an important role in maintaining replication (35), we employed DNA combing assays (50) and examined the acute effects of PARPis on replication fork movement. Nascent DNA was sequentially labeled with CldU and IdU for 30 min each with the PARPis (talazoparib, olaparib and veliparib) with differential PARP trapping ability, were added during the IdU pulse (Figure 4A). Consistent with previous studies (35,56), in the absence of PARPis, reduced fork progression was observed in *SPRTN*$^{-/-}$ TK6 cells as evidenced by decreased CldU tract lengths in *SPRTN*$^{-/-}$ TK6 cells in comparison with *wild-type* cells (Figure 4B). Low dose of talazoparib for a short time (30 min) caused a significant reduction of replication fork progression in *wild-type* cells as evidenced by reduced ratios of IdU- and CldU-labeled tract lengths (Figure 4C, compare lanes 1 and 4). A moderate but significant defects of replication fork progression was also observed in *wild-type* cells after short term olaparib, a less potent PARP trapper than talazoparib, treatment (12,25) (Figure 4C, compare lanes 1 and 3). Notably, the weak PARP trapper veliparib (12) did not impact replication fork progression in *wild-type* cells (Figure 4C, compare lanes 1 and 2).

SPRTN$^{-/-}$ cells displayed a stronger reduction (1.8-fold) in replication fork progression in response to talazoparib in comparison with *wild-type* cells (Figure 4C, compare lanes 4 and 8), while olaparib had a milder impact and veliparib did not affect replication fork progression in SPRTN-deficient cells (Figure 4C, compare lanes 5 and 6,7). These data show that replication fork stalling is correlated with the trapping potential of PARPis. Furthermore, the additive effects of SPRTN and talazoparib on replication fork suppression were eliminated by PARP1 deletion in SPRTN-deficient cells (Figure 4D), consistent with the conclusion that acute replication fork stalling in SPRTN-deficient cells upon PARPis treatment results from PARP1 trapping.

We next assessed whether the metalloprotease activity of SPRTN is important for maintaining replication fork progression upon talazoparib treatment. Ectopic expression of SPRTN WT rescued replication progression in SPRTN-deficient cells whereas expression of catalytic-dead SPRTN E112A was ineffective (Figure 4E). These results demonstrate the importance of SPRTN in preventing the stalling of replication forks by PARP trapping during replication.

We also performed DNA combing assays in *wild-type* and *SPRTN* KO cells in which forks were completely blocked using a prolonged exposure with hydroxyurea (HU) (2 mM for 2 h), followed by removal of HU and release in fresh medium in the presence and absence of talazoparib (Supplementary Figure S4A). *SPRTN* KO TK6 cells showed similar fork restart when compared to *wild-type* (∼80%) indicating that SPRTN alone had no effect on the resumption of DNA synthesis. Upon talazoparib treatment, *wild-type* cells displayed a marked decrease in the extent of fork restart (∼60%) and SPRTN depletion had no additional impact on fork restart (Supplementary Figure S4B).

SPRTN recruitment and interaction with PARP1 upon PARP trapping

Given that ectopically expressed SPRTN has been shown to form nuclear foci in response to UV and formaldehyde (57–59), we examined the recruitment of EGFP-tagged SPRTN upon talazoparib treatment by immunofluorescence microscopy in U2OS cells, which are amenable to this type of experiments. Significant accumulation of SPRTN foci was seen after treatment with talazoparib (Figure 5A and B), although the level of SPRTN expression in the nucleoplasm was similar in cells before and after talazoparib treatment (Supplementary Figure S5A). Notably, replication inhibition by aphidicolin during talazoparib treatment reduced significantly the SPRTN-EGFP foci (Figure 5B). Also, consistent with the coupling of SPRTN with replication, EGFP-SPRTN nuclear foci colocalized with the replication marker CDC45 (52) in S-phase cells upon talazoparib treatment (Figure 5C).

We next asked whether SPRTN interacts with PARP1. Chromatin immunoprecipitation experiments revealed that

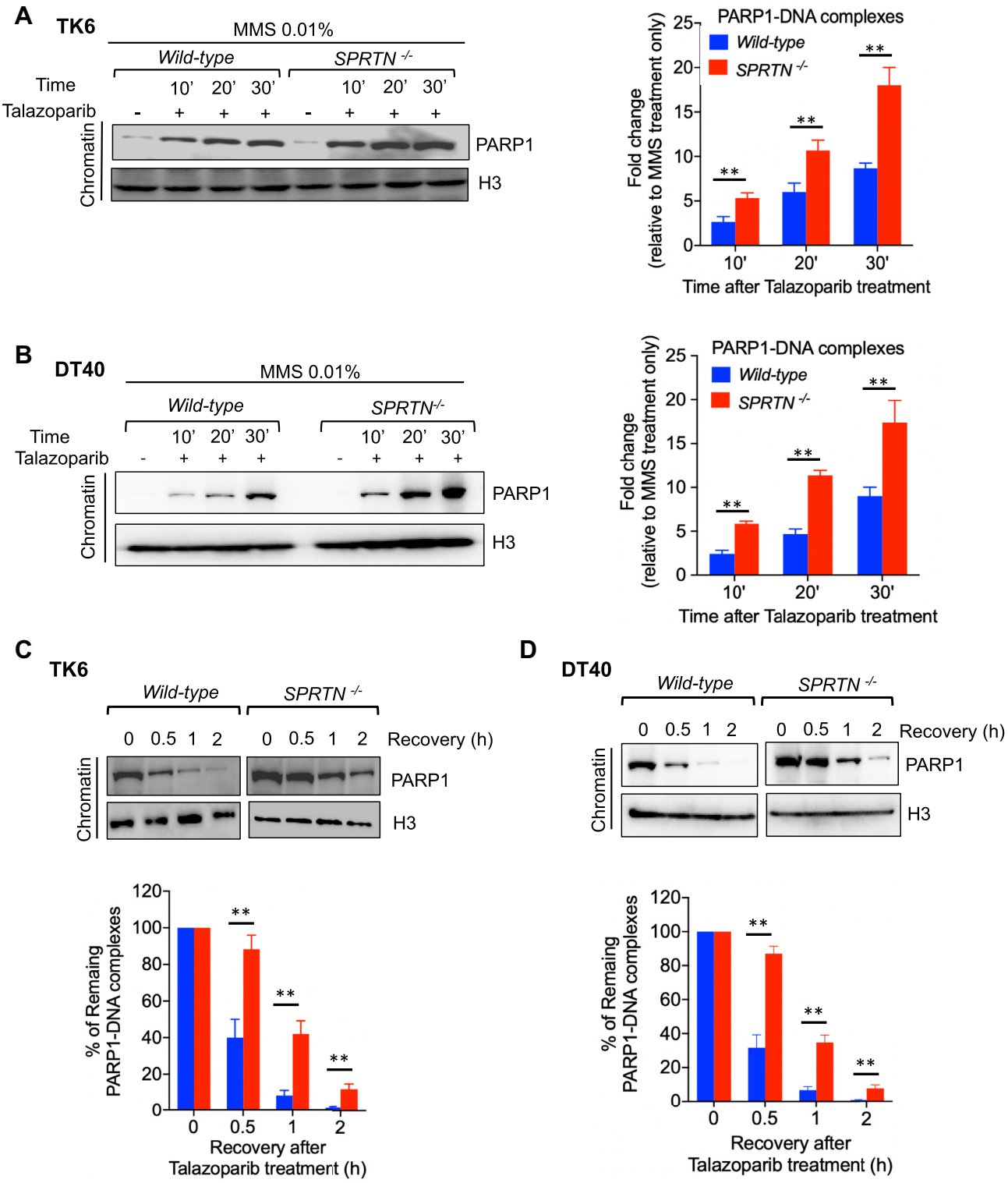

Figure 3. SPRTN releases trapped PARP1. (**A** and **B**) *Left panels*: Western blot of chromatin-bound fractions prepared from the indicated genotypes of human TK6 (A) and chicken DT40 (B) clones. Cells were treated with MMS (0.01%) and/or talazoparib (10 nM) for the indicated times. Blots were probed with the indicated antibodies. *Right panels*: Quantitation from the left panels of A and B. The histograms show the intensity of PARP1 signals relative to H3 signals. Error bars represent the SE from three independent experiments. $^{**}P < 0.01$ was considered significant (unpaired *t*-test). (**C** and **D**) *Top panels*: Representative Western blots of chromatin fractions from TK6 (C) and DT40 (D) cells probed with the indicated antibodies. Cells were treated with MMS (0.01%) and talazoparib (10 nM) for 30 min and released into a drug-free medium for the indicated times. The header indicates cell genotype and the length of time in hours in drug-free culture medium. *Bottom panels*: Bar plots of quantitative data from the top panels of C and D. Error bars represent the SE from three independent experiments. $^{**}P < 0.01$ was considered significant (unpaired *t*-test).

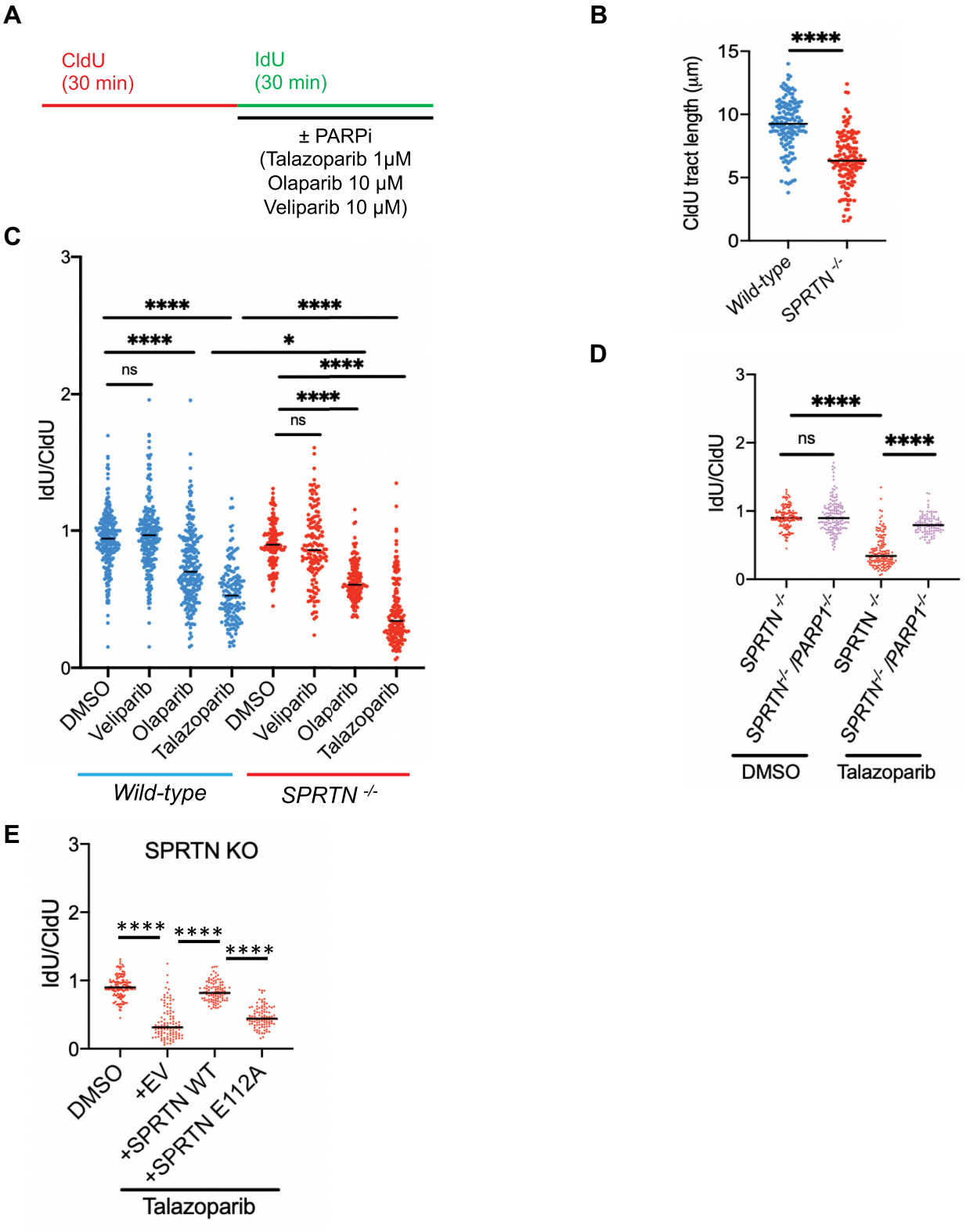

Figure 4. SPRTN limits replication fork stalling produced by PARP trapping. (**A**) Schematic representation of the DNA combing assay protocol. Nascent DNA was labeled with CldU (30 min) followed by IdU (30 min). PARPis at indicated concentrations were added together with IdU. (**B**) Dot plot showing the length of nascent DNA labeled by CldU in *wild-type* and *SPRTN*$^{-/-}$ TK6 cells. The distribution of replication tract lengths is shown. (**C**) *Wild-type* and *SPRTN* KO TK6 were treated with PARPis as indicated in panel A during IdU labeling. The distribution of replication forks at different IdU/CldU ratios is shown. (**D**) IdU/CldU ratios for the indicated genotypes are shown after treatment with either DMSO or 1 μM of talazoparib during IdU labeling. (**E**) *SPRTN* KO TK6 cells stably transfected with plasmids expressing SPRTN WT and SPRTN E112A (metalloprotease-dead mutant) were treated with 1 μM talazoparib. The distribution of replication forks is shown as IdU/CldU ratios. Horizontal black lines indicate median values and p-values were obtained by two-tailed unpaired *t*-test (*$P < 0.05$, ****$P < 0.0001$; ns = not significant).

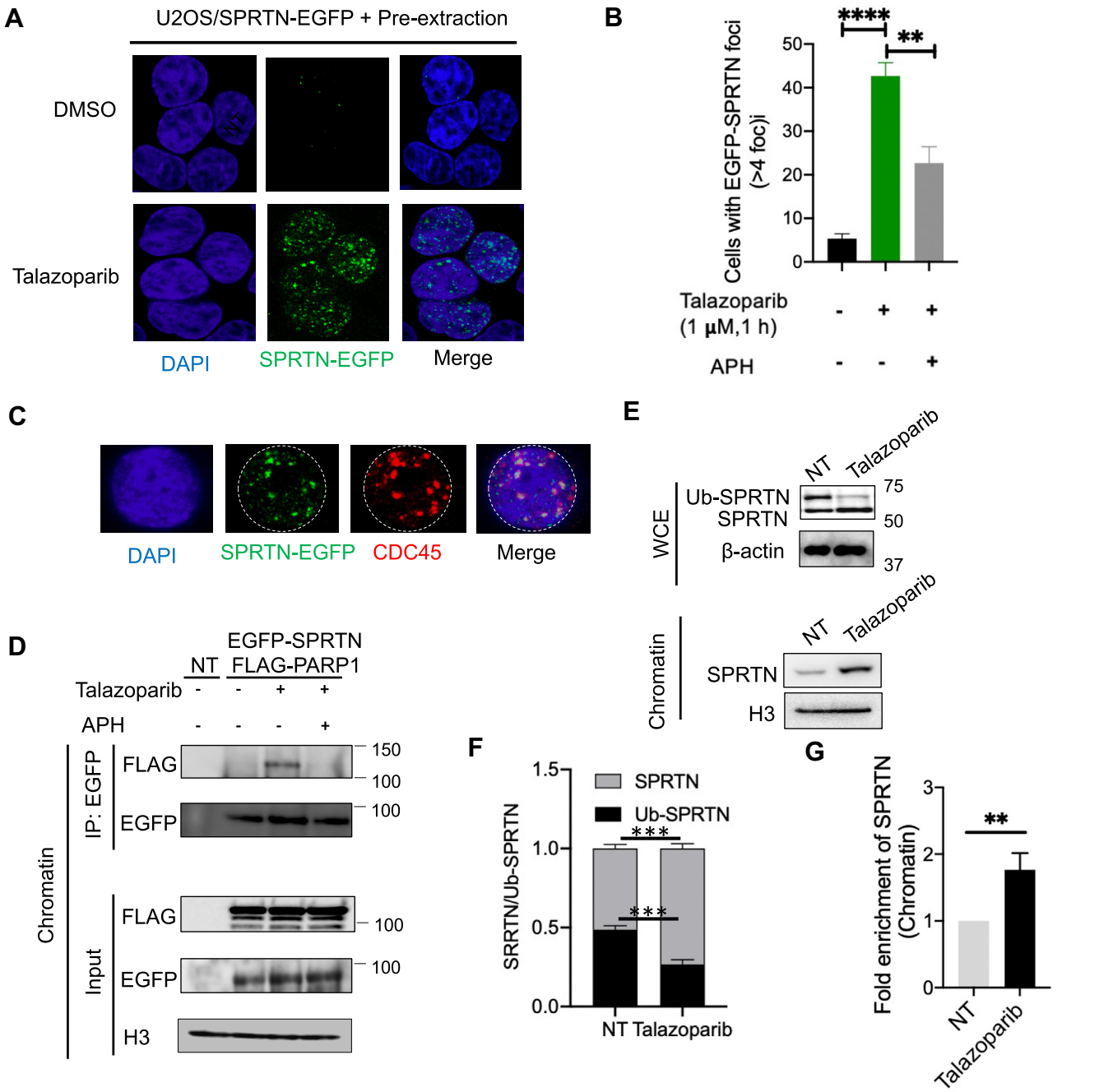

Figure 5. SPRTN is recruited to chromatin and interacts with PARP1 upon PARPi treatment in U2OS cells. (**A**) Cells expressing EGFP-SPRTN and exposed to talazoparib (1 μM) for 1 h were pre-extracted, fixed and analyzed by microscopy. Representative images are shown. (**B**) Quantification of data from experiments as shown in panel A (mean ± SD; at least 100 cells quantified per condition per experiment; $n = 3$ independent experiments). Quantification of nuclear EGFP-SPRTN foci is also shown when cells were pretreated with 1 μM APH for 30 min followed by co-treatment with talazoparib for 1 h. *P*-values were obtained by two-tailed unpaired *t*-test. $^{**}P < 0.01$, $^{****}P < 0.0001$. (**C**) Representative images of cells displaying SPRTN co-localization with CDC45. (**D**) Cells transfected both with EGFP-SPRTN and FLAG-PARP1 were pretreated with APH for 30 min followed by co-treatment with talazoparib for 30 min. GFP immunoprecipitation (IP) under denaturing conditions was followed by immunoblotting with FLAG and GFP antibodies. Cells were lysed and chromatin fractions were immunoprecipitated with S-protein agarose beads. Immunoblotting was performed with the indicated antibodies. (**E**) Cells were treated with talazoparib (1 μM) for 1 h. Whole cell lysates (top panel) and chromatin fractions (bottom panel) were immunoblotted with the indicated antibodies. (F) Bar graph showing the fraction of unmodified and monoubiquitinated SPRTN, quantified from blot in top panel E. The value of total SPRTN (unmodified and monoubiquitinated SPRTN) was considered as 1. Error bar indicates the mean value ± SE and P values were obtained by multiple unpaired *t*-test ($^{***}P < 0.001$). (**G**) Quantification of SPRTN fold-enrichment in chromatin after treatment with talazoparib for 1 h. The data were obtained from experiments shown at the bottom of panel E. Error bar indicates the mean value ± SD and *P* values were obtained by two-tailed unpaired *t*-test ($^{**}P < 0.01$).

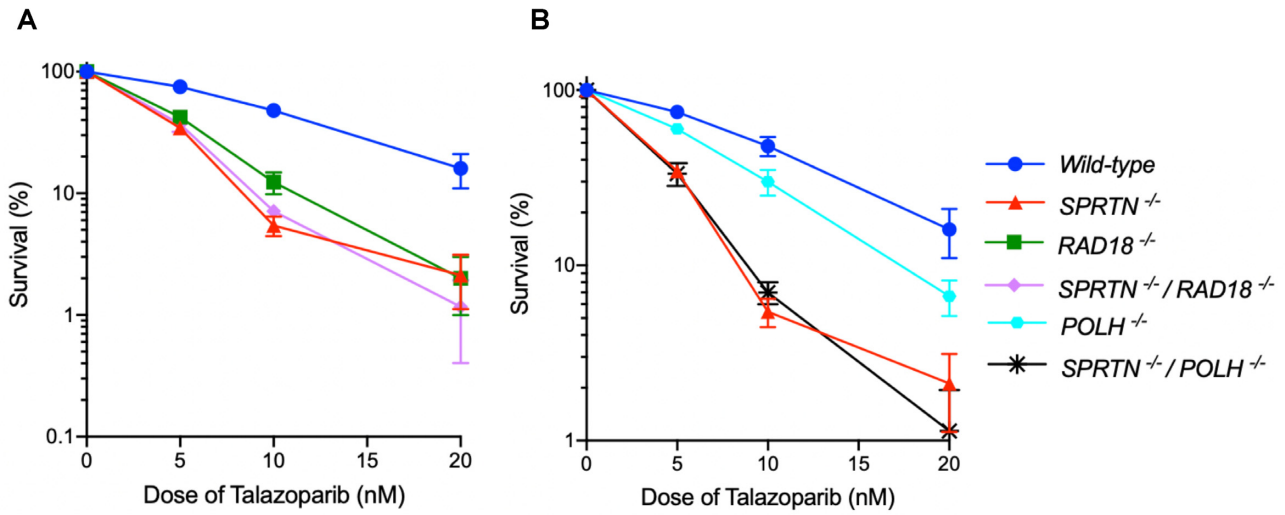

Figure 6. SPRTN is epistatic with the TLS-related genes RAD18 and POLH. (**A** and **B**) Colony survival of chicken DT40 cells with the indicated genotypes following exposure to talazoparib. The concentration of talazoparib is displayed on the x-axis on a linear scale, while the percentage of surviving cells is displayed on the y-axis on logarithmic scale. Error bars show the SD of the mean for three independent experiments. Percent survival was calculated as the percentage of surviving drug-treated cells relative to untreated cells.

ectopically expressed EGFP-tagged SPRTN interacted with PARP1 in the presence of talazoparib (Figure 5D). In addition, pretreatment with aphidicolin abolished talazoparib-induced interaction of SPRTN with PARP1 (Figure 5D), suggesting that SPRTN interacts with PARP1 via replication-dependent mechanisms.

Because formaldehyde-induced DPCs result in the deubiquitination of monoubiquitinated SPRTN allowing its recruitment to chromatin (43), we examined the deubiquitination of endogenous SPRTN in U2OS cells in response to talazoparib and observed it upon talazoparib treatment (Figure 5E, top panel, F). Because the unmodified fraction of SPRTN was also increased by talazoparib, we examined the levels of SPRTN without and after talazoparib treatment using chromatin fraction of *wild-type* cells where only the unmodified SPRTN was detected (Figure 5E, bottom panel), Increased SPRTN levels were observed upon talazoparib treatment (Figure 5E, bottom panel and G), suggesting that regulatory mechanisms control SPRTN activity or access to chromatin upon PARP trapping. A recent report also suggests that USP7 is the deubiquitylating enzyme (DUB) inducing the chromatin access of SPRTN upon DPC induction (60). Considering the essentiality of USP7 for DNA replication, we tested the effect of USP7 inhibition on SPRTN recruitment to chromatin after PARPi treatment and found that USP7 inhibition partially suppressed the chromatin recruitment of SPRTN upon talazoparib treatment (Supplementary Figure S5B). Taken together, these data support the involvement of SPRTN in response to PARP1 trapping.

SPRTN and the TLS pathway are epistatic in response to PARP inhibitor treatment

Translesion DNA synthesis (TLS) is important to bypass DPC-induced bulky DNA lesions (1,44). The TLS pathway-related proteins have also been shown to be produce cellular tolerance to PARPis in vertebrate cells as evidenced by the hypersensitivity of DT40 RAD18- and POLH-deficient cells to PARPi (11). The cellular sensitivity of *RAD18*$^{-/-}$ DT40 cells to PARPi has been proposed to be derived from the trapping of PARP-DNA complexes (11). In addition to its DPC protease activity, SPRTN has been implicated as a regulator of TLS (61). This led us to ask whether SPRTN and TLS proteins such as RAD18 act in the same pathway by performing colony survival assays. *SPRTN*$^{-/-}$/*RAD18*$^{-/-}$ double KO cells exhibited similar talazoparib sensitivity as the *SPRTN*$^{-/-}$or *RAD18*$^{-/-}$ single KO cells (Figure 6A), suggesting that SPRTN and RAD18 are epistatic. *SPRTN*$^{-/-}$/*POLH*$^{-/-}$ cells also displayed similar talazoparib sensitivity as the *SPRTN*$^{-/-}$ cells although *POLH*$^{-/-}$cells showed mild sensitivity to talazoparib (Figure 6B). These results suggest an epistatic relationship between SPRTN and TLS in addition to the proteolytic function of SPRTN for the removal of trapped PARP1.

DISCUSSION

SPRTN has recently been implicated as a replication-associated protease for the repair of DPCs induced by formaldehyde and by the trapping of TOP1 and TOP2 by anticancer drugs and DNA alterations (10,35,38,43,55). Here we report that SPRTN is also involved in the repair of PARP1–DNA complexes induced by the clinically used anticancer PARPis talazoparib and olaparib. We show in two cell line models (human TK6 and chicken DT40 cells) that the removal of trapped PARP1 is dependent on SPRTN as evidenced by the slower repair kinetics of PARP1–DNA complexes in the chromatin fraction of *SPRTN* KO cells and the complementation by SPRTN transfection. We propose a model (Figure 7) for the role of SPRTN in the completion of replication in PARP1–DNA complexes-containing chromatin and for the role of SPRTN in conferring resistance of cancer cells to PARPis.

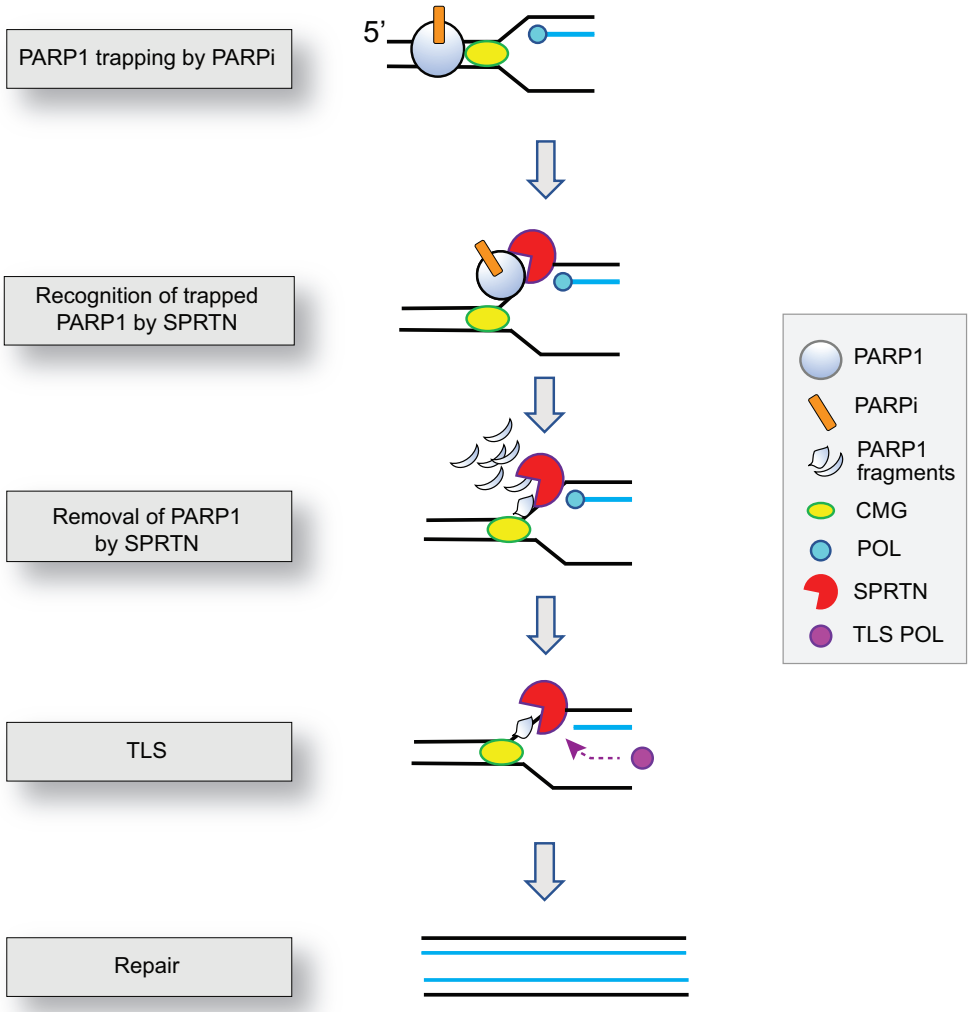

Figure 7. Model for PARP1–DNA complex repair by SPRTN. Trapping of PARP1 at replication forks induces the recruitment of SPRTN and the debulking of PARP1–DNA complexes by SPRTN. Peptide remnants linked to DNA may require SPRTN-associated translesion synthesis (TLS) polymerases for replication completion. POL: Replicative DNA polymerases.

DNA fiber analyses revealed that loss of SPRTN leads to a significantly reduction of replication fork movement even in the absence of drug treatment (Figure 4B), which highlights the importance of SPRTN for normal replication and for potentially eliminating endogenous DPCs at replication forks. Reduced fork progression could also be detected after acute treatment with PARP trappers with ∼2-fold shortening of the mean second track length in the *SPRTN* KO cells (Figure 4C), suggesting the role of SPRTN in resolving PARP1–DNA complexes associated with replication. This observation is consistent with the previous finding that SPRTN-deficient cells exhibit reduced replication fork progression when challenged by the DPC-inducing agents formaldehyde and camptothecin (35). Notably, we find that the negative impact of PARPis on replication fork extension is correlated with the trapping potency of three clinical PARPis (talazoparib, olaparib and veliparib) (11,12,25) in *wild-type* and SPRTN-deficient cells (Figure 4C), suggesting that trapped PARP can act as a source of replication blockage and/or stress. Together, our results suggest that SPRTN regulates replication fork progression and prevents the accumulation of abortive PARP1–DNA complexes at sites of DNA replication. Consistently, we found greater accumulation of trapped PARP1 in the chromatin in *SPRTN* KO lymphoblastoid TK6 and DT40 cells after PARPi treatment (Figure 3 and Supplementary Figure S3).

Previous studies suggested that the cell killing mechanisms by PARP inhibitors is primarily due to PARP trapping and DNA damage rather than catalytic inhibition of PARP (11,12,25). In this study, we show that inhibiting ongoing DNA replication by aphidicolin protected against the cytotoxicity of talazoparib. This highlights the implication of active replication is as a DNA damaging determinant of PARP trapping with DNA (Figure 1D). Accordingly, we could detect PARP1 in chromatin fractions after SPRTN pull-down following talazoparib treatment and found that trapped PARP1 was reduced upon replication inhibition by aphidicolin (Figure 5D).

A recent study implicated the serine protease FAM111A (FAMily with sequence similarity 111 member A), and

not SPRTN for the repair of PARP1–DNA complexes to ensure replication fork progression in human haploid leukemia HAP1 cells (62). Consistently, another study by the same group reported that SPRTN hypomorphic murine embryonic fibroblast (MEF) cells were not hypersensitive to PARPis (38). The apparent discrepancy regarding the implication of SPRTN between our results and these observations might be explained by cell-type specific difference as SPRTN and FAM111A are not equally expressed in different cell lines and some cancer cell lines fail to express SPRTN or FAM111A (https://discover.nci.nih.gov/cellminercdb/); also, residual level of SPRTN protein in hypomorphic SPRTN cells might be sufficient to resolve trapped PARP-DNA complexes.

The chromatin remodeling helicase ALC1/CHD1L has also been reported as regulating the removal or release of chromatin-bound PARP1, and as a determinant of PARPi cytotoxicity in HR-deficient cells (63,64). Moreover, PARPis have been shown to modulate ALC1 level by decreasing its ubiquitination (65). Yet, a recent report concluded that ALC1 catalyzes the release of PARP2, not PARP1, which in turn affects the DDR and PARPi potency (66). Hence, further studies are warranted to determine the potential interactions of ALC1 and SPRTN with respect to PARP trapping.

In summary, we propose a model in which the encounter of SPRTN with trapped PARP1 at replication forks leads to SPRTN activation and to the debulking of chromatin-trapped PARP1 to ensure replication fork progression (Figure 7). In addition, we provide evidence (11,29) that TLS pathway-related mutants in mammalian cells are sensitive to PARPis (Figure 6A and B). If the remnant PARP1 was still bound to DNA after proteolytic digestion by SPRTN, an important question is how cells process DNA-peptide complexes resulting from the proteolytic degradation or debulking of PARP1–DNA complexes. Previous studies in yeast and *Xenopus* egg extracts suggest the involvement of TLS polymerase ζ to bypass remaining DNA-peptide crosslinks after DPC proteolysis *in vivo* and *in vitro*, respectively (67,68). Moreover, it was reported that SPRTN and RAD18 work together in protecting human cells TLS against formaldehyde induced DPCs (34). Here, we provide genetic evidence of epistasis of SPRTN- and TLS-related pathway proteins in vertebrate cells for cellular tolerance to PARPis.

We also observed a potential link of USP7 and SPRTN upon PARP trapping (Supplementary Figure S5B). However, future studies will be required to understand how SPRTN is deubiquitinated and activated by PARP trapping. Also, whether and how SPRTN itself helps in recruiting TLS polymerases remains to be investigated. Indeed, previous studies indicated that SPRTN can facilitate the recruitment of Polη in the replication fork (59,69). Perhaps DNA polymerase ε can be exchanged by TLS polymerases for the bypass of PARP1–DNA complexes lesions where short peptides of PARP1 still remain attached to DNA (Figure 7), which is the case for formaldehyde-induced DPCs (34). In conclusion, our study extends the role of SPRTN to a wide range of chromatin-bound proteins targeted by anticancer agents such as PARP and topoisomerases.

SUPPLEMENTARY DATA

Supplementary Data are available at NAR Online.

ACKNOWLEDGEMENTS

We thank Professor Lee Zou (Harvard Medical School, Massachusetts General Hospital Cancer Center) for providing EGFP tagged human SPRTN WT plasmid construct as a gift. We are also thankful to microscopy core facility, Center for Cancer Research (CCR), NCI, NIH for imaging.

FUNDING

Center for Cancer Research; Intramural Program of the National Cancer Institute, National Institutes of Health, Bethesda, Maryland 20892 [Z01 BC Z01 BC 006161-17, Z01 BC 006150-19 to Y.P.]; JSPS KAKENHI [16H12595, 16H06306 to S.T.]; JSPS Core-to-Core Program, A. Advanced Research Networks (to S.T.). Funding for open access charge: National Institutes of Health [Z01 BC Z01 BC 006161-17, Z01 BC 006150-19].
Conflict of interest statement. None declared.

REFERENCES

1. Stingele,J., Habermann,B. and Jentsch,S. (2015) DNA–protein crosslink repair: proteases as DNA repair enzymes. *Trends Biochem. Sci.*, **40**, 67–71.
2. Kojima,Y. and Machida,Y.J. (2020) DNA-protein crosslinks from environmental exposure: mechanisms of formation and repair. *Environ. Mol. Mutagen.*, **61**, 716–729.
3. Quinones,J.L., Thapar,U., Yu,K., Fang,Q., Sobol,R.W. and Demple,B. (2015) Enzyme mechanism-based, oxidative DNA–protein cross-links formed with DNA polymerase beta in vivo. *Proc. Natl. Acad. Sci. U.S.A.*, **112**, 8602–8607.
4. Prasad,R., Horton,J.K., Dai,D.P. and Wilson,S.H. (2019) Repair pathway for PARP-1 DNA–protein crosslinks. *DNA Repair (Amst.)*, **73**, 71–77.
5. Piersen,C.E., Prasad,R., Wilson,S.H. and Lloyd,R.S. (1996) Evidence for an imino intermediate in the DNA polymerase beta deoxyribose phosphate excision reaction. *J. Biol. Chem.*, **271**, 17811–17815.
6. Hsiang,Y.H., Hertzberg,R., Hecht,S. and Liu,L.F. (1985) Camptothecin induces protein-linked DNA breaks via mammalian DNA topoisomerase I. *J. Biol. Chem.*, **260**, 14873–14878.
7. Pommier,Y. and Marchand,C. (2011) Interfacial inhibitors: targeting macromolecular complexes. *Nat. Rev. Drug Discov.*, **11**, 25–36.
8. Nitiss,J.L. (2009) Targeting DNA topoisomerase II in cancer chemotherapy. *Nat. Rev. Cancer*, **9**, 338–350.
9. Maslov,A.Y., Lee,M., Gundry,M., Gravina,S., Strogonova,N., Tazearslan,C., Bendebury,A., Suh,Y. and Vijg,J. (2012) 5-aza-2'-deoxycytidine-induced genome rearrangements are mediated by DNMT1. *Oncogene*, **31**, 5172–5179.
10. Sun,Y., Saha,L.K., Saha,S., Jo,U. and Pommier,Y. (2020) Debulking of topoisomerase DNA–protein crosslinks (TOP-DPC) by the proteasome, non-proteasomal and non-proteolytic pathways. *DNA Repair (Amst.)*, **94**, 102926.
11. Murai,J., Huang,S.-y.N., Das,B.B., Renaud,A., Zhang,Y., Doroshow,J.H., Ji,J., Takeda,S. and Pommier,Y. (2012) Trapping of PARP1 and PARP2 by Clinical PARP Inhibitors. *Cancer Res.*, **72**, 5588–5599.
12. Pommier,Y., O'Connor,M.J. and de Bono,J. (2016) Laying a trap to kill cancer cells: PARP inhibitors and their mechanisms of action. *Sci. Transl. Med.*, **8**, 362ps317.
13. Ray Chaudhuri,A. and Nussenzweig,A. (2017) The multifaceted roles of PARP1 in DNA repair and chromatin remodelling. *Nat. Rev. Mol. Cell Biol.*, **18**, 610–621.
14. Anachkova,B., Russev,G. and Poirier,G.G. (1989) DNA replication and poly(ADP-ribosyl)ation of chromatin. *Cytobios*, **58**, 19–28.

15. Lehmann,A.R., Kirk-Bell,S., Shall,S. and Whish,W.J. (1974) The relationship between cell growth, macromolecular synthesis and poly ADP-ribose polymerase in lymphoid cells. *Exp. Cell Res.*, **83**, 63–72.
16. Yung,T.M., Sato,S. and Satoh,M.S. (2004) Poly(ADP-ribosyl)ation as a DNA damage-induced post-translational modification regulating poly(ADP-ribose) polymerase-1-topoisomerase I interaction. *J. Biol. Chem.*, **279**, 39686–39696.
17. Bryant,H.E., Petermann,E., Schultz,N., Jemth,A.S., Loseva,O., Issaeva,N., Johansson,F., Fernandez,S., McGlynn,P. and Helleday,T. (2009) PARP is activated at stalled forks to mediate Mre11-dependent replication restart and recombination. *EMBO J.*, **28**, 2601–2615.
18. Dantzer,F., Nasheuer,H.P., Vonesch,J.L., de Murcia,G. and Menissier-de Murcia,J. (1998) Functional association of poly(ADP-ribose) polymerase with DNA polymerase alpha-primase complex: a link between DNA strand break detection and DNA replication. *Nucleic Acids Res.*, **26**, 1891–1898.
19. Simbulan-Rosenthal,C.M., Rosenthal,D.S., Boulares,A.H., Hickey,R.J., Malkas,L.H., Coll,J.M. and Smulson,M.E. (1998) Regulation of the expression or recruitment of components of the DNA synthesome by poly(ADP-ribose) polymerase. *Biochemistry*, **37**, 9363–9370.
20. Hanzlikova,H., Kalasova,I., Demin,A.A., Pennicott,L.E., Cihlarova,Z. and Caldecott,K.W. (2018) The importance of poly(ADP-ribose) polymerase as a sensor of unligated Okazaki fragments during DNA replication. *Mol. Cell*, **71**, 319–331.
21. Sugimura,K., Takebayashi,S., Taguchi,H., Takeda,S. and Okumura,K. (2008) PARP-1 ensures regulation of replication fork progression by homologous recombination on damaged DNA. *J. Cell Biol.*, **183**, 1203–1212.
22. Yang,Y.G., Cortes,U., Patnaik,S., Jasin,M. and Wang,Z.Q. (2004) Ablation of PARP-1 does not interfere with the repair of DNA double-strand breaks, but compromises the reactivation of stalled replication forks. *Oncogene*, **23**, 3872–3882.
23. Berti,M., Ray Chaudhuri,A., Thangavel,S., Gomathinayagam,S., Kenig,S., Vujanovic,M., Odreman,F., Glatter,T., Graziano,S., Mendoza-Maldonado,R. *et al.* (2013) Human RECQ1 promotes restart of replication forks reversed by DNA topoisomerase I inhibition. *Nat. Struct. Mol. Biol.*, **20**, 347–354.
24. Genois,M.M., Gagne,J.P., Yasuhara,T., Jackson,J., Saxena,S., Langelier,M.F., Ahel,I., Bedford,M.T., Pascal,J.M., Vindigni,A. *et al.* (2020) CARM1 regulates replication fork speed and stress response by stimulating PARP1. *Mol. Cell*, **81**, 784–800.
25. Murai,J., Huang,S.Y., Renaud,A., Zhang,Y., Ji,J., Takeda,S., Morris,J., Teicher,B., Doroshow,J.H. and Pommier,Y. (2014) Stereospecific PARP trapping by BMN 673 and comparison with olaparib and rucaparib. *Mol. Cancer Ther.*, **13**, 433–443.
26. Zandarashvili,L., Langelier,M.F., Velagapudi,U.K., Hancock,M.A., Steffen,J.D., Billur,R., Hannan,Z.M., Wicks,A.J., Krastev,D.B., Pettitt,S.J. *et al.* (2020) Structural basis for allosteric PARP-1 retention on DNA breaks. *Science*, **368**, eaax6367.
27. Farmer,H., McCabe,N., Lord,C.J., Tutt,A.N., Johnson,D.A., Richardson,T.B., Santarosa,M., Dillon,K.J., Hickson,I., Knights,C. *et al.* (2005) Targeting the DNA repair defect in BRCA mutant cells as a therapeutic strategy. *Nature*, **434**, 917–921.
28. Bryant,H.E., Schultz,N., Thomas,H.D., Parker,K.M., Flower,D., Lopez,E., Kyle,S., Meuth,M., Curtin,N.J. and Helleday,T. (2005) Specific killing of BRCA2-deficient tumours with inhibitors of poly(ADP-ribose) polymerase. *Nature*, **434**, 913–917.
29. Murai,J. and Pommier,Y. (2019) PARP trapping beyond homologous recombination and platinum sensitivity in cancers. *Annu. Rev. Cancer Biol.*, **3**, 131–150.
30. Prasad,R., Horton,J.K., Chastain,P.D. 2nd, Gassman,N.R., Freudenthal,B.D., Hou,E.W. and Wilson,S.H. (2014) Suicidal cross-linking of PARP-1 to AP site intermediates in cells undergoing base excision repair. *Nucleic Acids Res.*, **42**, 6337–6351.
31. Ma,A. and Dai,X. (2018) The relationship between DNA single-stranded damage response and double-stranded damage response. *Cell Cycle*, **17**, 73–79.
32. Menon,V. and Povirk,L. (2014) Involvement of p53 in the repair of DNA double strand breaks: multifaceted Roles of p53 in homologous recombination repair (HRR) and non-homologous end joining (NHEJ). *Subcell. Biochem.*, **85**, 321–336.
33. Larsen,N.B., Gao,A.O., Sparks,J.L., Gallina,I., Wu,R.A., Mann,M., Raschle,M., Walter,J.C. and Duxin,J.P. (2019) Replication-coupled DNA-protein crosslink repair by SPRTN and the proteasome in xenopus egg extracts. *Mol. Cell*, **73**, 574–588.
34. Morocz,M., Zsigmond,E., Toth,R., Enyedi,M.Z., Pinter,L. and Haracska,L. (2017) DNA-dependent protease activity of human Spartan facilitates replication of DNA–protein crosslink-containing DNA. *Nucleic Acids Res.*, **45**, 3172–3188.
35. Vaz,B., Popovic,M., Newman,J.A., Fielden,J., Aitkenhead,H., Halder,S., Singh,A.N., Vendrell,I., Fischer,R., Torrecilla,I. *et al.* (2016) Metalloprotease SPRTN/DVC1 orchestrates replication-coupled DNA-protein crosslink repair. *Mol. Cell*, **64**, 704–719.
36. Lessel,D., Vaz,B., Halder,S., Lockhart,P.J., Marinovic-Terzic,I., Lopez-Mosqueda,J., Philipp,M., Sim,J.C., Smith,K.R., Oehler,J. *et al.* (2014) Mutations in SPRTN cause early onset hepatocellular carcinoma, genomic instability and progeroid features. *Nat. Genet.*, **46**, 1239–1244.
37. Ruijs,M.W., van Andel,R.N., Oshima,J., Madan,K., Nieuwint,A.W. and Aalfs,C.M. (2003) Atypical progeroid syndrome: an unknown helicase gene defect? *Am. J. Med. Genet. A*, **116A**, 295–299.
38. Maskey,R.S., Flatten,K.S., Sieben,C.J., Peterson,K.L., Baker,D.J., Nam,H.J., Kim,M.S., Smyrk,T.C., Kojima,Y., Machida,Y. *et al.* (2017) Spartan deficiency causes accumulation of Topoisomerase 1 cleavage complexes and tumorigenesis. *Nucleic Acids Res.*, **45**, 4564–4576.
39. Hart,T., Chandrashekhar,M., Aregger,M., Steinhart,Z., Brown,K.R., MacLeod,G., Mis,M., Zimmermann,M., Fradet-Turcotte,A., Sun,S. *et al.* (2015) High-resolution CRISPR screens reveal fitness genes and genotype-specific cancer liabilities. *Cell*, **163**, 1515–1526.
40. Wang,T., Birsoy,K., Hughes,N.W., Krupczak,K.M., Post,Y., Wei,J.J., Lander,E.S. and Sabatini,D.M. (2015) Identification and characterization of essential genes in the human genome. *Science*, **350**, 1096–1101.
41. Reinking,H.K., Kang,H.S., Gotz,M.J., Li,H.Y., Kieser,A., Zhao,S., Acampora,A.C., Weickert,P., Fessler,E., Jae,L.T. *et al.* (2020) DNA structure-specific cleavage of DNA-protein crosslinks by the SPRTN protease. *Mol. Cell*, **80**, 102–113.
42. Li,F., Raczynska,J.E., Chen,Z. and Yu,H. (2019) Structural Insight into DNA-dependent activation of human metalloprotease spartan. *Cell Rep.*, **26**, 3336–3346.
43. Stingele,J., Bellelli,R., Alte,F., Hewitt,G., Sarek,G., Maslen,S.L., Tsutakawa,S.E., Borg,A., Kjaer,S., Tainer,J.A. *et al.* (2016) Mechanism and regulation of DNA-protein crosslink repair by the DNA-dependent metalloprotease SPRTN. *Mol. Cell*, **64**, 688–703.
44. Stingele,J., Bellelli,R. and Boulton,S.J. (2017) Mechanisms of DNA–protein crosslink repair. *Nat. Rev. Mol. Cell Biol.*, **18**, 563–573.
45. Prasad,R., Horton,J.K. and Wilson,S.H. (2020) Requirements for PARP-1 covalent crosslinking to DNA (PARP-1 DPC). *DNA Repair (Amst.)*, **90**, 102850.
46. Hu,Q., Klages-Mundt,N., Wang,R., Lynn,E., Kuma Saha,L., Zhang,H., Srivastava,M., Shen,X., Tian,Y., Kim,H. *et al.* (2020) The ARK assay is a sensitive and versatile method for the global detection of DNA-protein crosslinks. *Cell Rep.*, **30**, 1235–1245.
47. Akagawa,R., Trinh,H.T., Saha,L.K., Tsuda,M., Hirota,K., Yamada,S., Shibata,A., Kanemaki,M.T., Nakada,S., Takeda,S. *et al.* (2020) UBC13-mediated ubiquitin signaling promotes removal of blocking adducts from DNA double-strand breaks. *iScience*, **23**, 101027.
48. Nakazato,A., Kajita,K., Ooka,M., Akagawa,R., Abe,T., Takeda,S., Branzei,D. and Hirota,K. (2018) SPARTAN promotes genetic diversification of the immunoglobulin-variable gene locus in avian DT40 cells. *DNA Repair (Amst.)*, **68**, 50–57.
49. Keka,I.S., Mohiuddin, Maede,Y., Rahman,M.M., Sakuma,T., Honma,M., Yamamoto,T., Takeda,S. and Sasanuma,H. (2015) Smarcal1 promotes double-strand-break repair by nonhomologous end-joining. *Nucleic Acids Res.*, **43**, 6359–6372.
50. Conti,C., Seiler,J. and Pommier,Y. (2007) The mammalian DNA replication elongation checkpoint: implication of Chk1 and relationship with origin firing as determined by single DNA molecule and single cell analyses. *Cell Cycle*, **6**, 2760–2767.
51. Seiler,J.A., Conti,C., Syed,A., Aladjem,M.I. and Pommier,Y. (2007) The intra-S-phase checkpoint affects both DNA replication initiation and elongation: single-cell and -DNA fiber analyses. *Mol. Cell. Biol.*, **27**, 5806–5818.

52. Murai,J., Tang,S.-W., Leo,E., Baechler,S.A., Redon,C.E., Zhang,H., Al Abo,M., Rajapakse,V.N., Nakamura,E., Jenkins,L.M.M. *et al.* (2018) SLFN11 blocks stressed replication forks independently of ATR. *Mol. Cell*, **69**, 371–384.
53. Saha,L.K., Wakasugi,M., Akter,S., Prasad,R., Wilson,S.H., Shimizu,N., Sasanuma,H., Huang,S.N., Agama,K., Pommier,Y. *et al.* (2020) Topoisomerase I-driven repair of UV-induced damage in NER-deficient cells. *Proc. Natl. Acad. Sci. U.S.A.*, **117**, 14412–14420.
54. Holm,C., Covey,J.M., Kerrigan,D. and Pommier,Y. (1989) Differential requirement of DNA replication for the cytotoxicity of DNA topoisomerase I and II inhibitors in Chinese hamster DC3F cells. *Cancer Res.*, **49**, 6365–6368.
55. Lopez-Mosqueda,J., Maddi,K., Prgomet,S., Kalayil,S., Marinovic-Terzic,I., Terzic,J. and Dikic,I. (2016) SPRTN is a mammalian DNA-binding metalloprotease that resolves DNA–protein crosslinks. *Elife*, **5**, e21491.
56. Halder,S., Torrecilla,I., Burkhalter,M.D., Popovic,M., Fielden,J., Vaz,B., Oehler,J., Pilger,D., Lessel,D., Wiseman,K. *et al.* (2019) SPRTN protease and checkpoint kinase 1 cross-activation loop safeguards DNA replication. *Nat. Commun.*, **10**, 3142.
57. Borgermann,N., Ackermann,L., Schwertman,P., Hendriks,I.A., Thijssen,K., Liu,J.C., Lans,H., Nielsen,M.L. and Mailand,N. (2019) SUMOylation promotes protective responses to DNA–protein crosslinks. *EMBO J.*, **38**, e101496.
58. Machida,Y., Kim,M.S. and Machida,Y.J. (2012) Spartan/C1orf124 is important to prevent UV-induced mutagenesis. *Cell Cycle*, **11**, 3395–3402.
59. Centore,R.C., Yazinski,S.A., Tse,A. and Zou,L. (2012) Spartan/C1orf124, a reader of PCNA ubiquitylation and a regulator of UV-induced DNA damage response. *Mol. Cell*, **46**, 625–635.
60. Zhao,S., Kieser,A., Li,H.Y., Reinking,H.K., Weickert,P., Euteneuer,S., Yaneva,D., Acampora,A.C., Gotz,M.J., Feederle,R. *et al.* (2021) A ubiquitin switch controls autocatalytic inactivation of the DNA–protein crosslink repair protease SPRTN. *Nucleic Acids Res.*, **49**, 902–915.
61. Kim,M.S., Machida,Y., Vashisht,A.A., Wohlschlegel,J.A., Pang,Y.P. and Machida,Y.J. (2013) Regulation of error-prone translesion synthesis by Spartan/C1orf124. *Nucleic Acids Res.*, **41**, 1661–1668.
62. Kojima,Y., Machida,Y., Palani,S., Caulfield,T.R., Radisky,E.S., Kaufmann,S.H. and Machida,Y.J. (2020) FAM111A protects replication forks from protein obstacles via its trypsin-like domain. *Nat. Commun.*, **11**, 1318.
63. Juhasz,S., Smith,R., Schauer,T., Spekhardt,D., Mamar,H., Zentout,S., Chapuis,C., Huet,S. and Timinszky,G. (2020) The chromatin remodeler ALC1 underlies resistance to PARP inhibitor treatment. *Sci. Adv.*, **6**, eabb8626.
64. Verma,P., Zhou,Y., Cao,Z., Deraska,P.V., Deb,M., Arai,E., Li,W., Shao,Y., Puentes,L., Li,Y. *et al.* (2021) ALC1 links chromatin accessibility to PARP inhibitor response in homologous recombination-deficient cells. *Nat. Cell Biol.*, **23**, 160–171.
65. Wang,Y., Wang,Y., Wang,N., You,L., Long,F., Shao,C., Wang,Y. and Wu,J. (2019) Poly(ADPribose) polymerase 1/2 inhibitors decrease the ubiquitination of ALC1 mediated by CHFR in breast cancer. *Oncol. Rep.*, **42**, 1467–1474.
66. Blessing,C., Mandemaker,I.K., Gonzalez-Leal,C., Preisser,J., Schomburg,A. and Ladurner,A.G. (2020) The oncogenic helicase ALC1 regulates PARP inhibitor potency by trapping PARP2 at DNA breaks. *Mol. Cell*, **80**, 862–875.
67. Stingele,J., Schwarz,M.S., Bloemeke,N., Wolf,P.G. and Jentsch,S. (2014) A DNA-dependent protease involved in DNA–protein crosslink repair. *Cell*, **158**, 327–338.
68. Duxin,J.P., Dewar,J.M., Yardimci,H. and Walter,J.C. (2014) Repair of a DNA–protein crosslink by replication-coupled proteolysis. *Cell*, **159**, 346–357.
69. Ghosal,G., Leung,J.W., Nair,B.C., Fong,K.W. and Chen,J. (2012) Proliferating cell nuclear antigen (PCNA)-binding protein C1orf124 is a regulator of translesion synthesis. *J. Biol. Chem.*, **287**, 34225–34233.